

# Ir-Sb Binary System: Unveiling Nodeless Unconventional Superconductivity Proximate to Honeycomb-Vacancy Ordering

V. Sazgari,<sup>1</sup> Tianping Ying,<sup>2,3</sup> J.N. Graham,<sup>1</sup> C. Mielke III,<sup>1</sup> D. Das,<sup>1</sup> S.S. Islam,<sup>1</sup>  
M. Bartkowiak,<sup>4</sup> R. Khasanov,<sup>1</sup> H. Luetkens,<sup>1</sup> H. Hosono,<sup>2</sup> and Z. Guguchia<sup>1,\*</sup>

<sup>1</sup>Laboratory for Muon Spin Spectroscopy, Paul Scherrer Institute, CH-5232 Villigen PSI, Switzerland

<sup>2</sup>Materials Research Center for Element Strategy,

Tokyo Institute of Technology, Yokohama 226-8503, Japan

<sup>3</sup>Beijing National Laboratory for Condensed Matter Physics,

Institute of Physics, Chinese Academy of Sciences, Beijing 100190, China

<sup>4</sup>Laboratory for Neutron and Muon Instrumentation,  
Paul Scherrer Institut, CH-5232 Villigen, Switzerland

Vacancies play a crucial role in solid-state physics, but their impact on materials with strong electron-electron correlations has been underexplored. A recent study on the Ir-Sb binary system,  $\text{Ir}_{16}\text{Sb}_{18}$  revealed a novel extended buckled-honeycomb vacancy (BHV) order [1, 2]. Superconductivity is induced by suppressing the BHV ordering through high-pressure growth with excess Ir atoms or isovalent Rh substitution, although the nature of superconducting pairing has remained unexplored. Here, we conduct muon spin rotation experiments probing the temperature-dependence of the effective magnetic penetration depth  $\lambda_{eff}(T)$  in  $\text{Ir}_{1-\delta}\text{Sb}$  (synthesized at 5.5 GPa with  $T_c = 4.2$  K) and ambient pressure synthesized optimally Rh-doped  $\text{Ir}_{1-x}\text{Rh}_x\text{Sb}$  ( $x=0.3$ ,  $T_c = 2.7$  K). The exponential temperature dependence of the superfluid density  $n_s/m^*$  at low temperatures indicates a fully gapped superconducting state in both samples. Notably, the ratio of  $T_c$  to the superfluid density is comparable to previously measured unconventional superconductors. A significant increase in  $n_s/m^*$  in the high-pressure synthesized sample correlates with  $T_c$ , a hallmark feature of unconventional superconductivity. This correlation is intrinsic to superconductivity in the Ir-Sb binary system, with the ratio of  $T_c$  and the Fermi temperature  $T_F$  about 20 times lower than in hole-doped cuprates. We further demonstrate a similar effect induced by chemical pressure (Rh substitution) and hydrostatic pressure in  $\text{Ir}_{1-x}\text{Rh}_x\text{Sb}$ , highlighting that the dome-shaped phase diagram is a fundamental feature of the material. These findings underscore the unconventional nature of the observed superconductivity, and classifies IrSb as the first unconventional superconducting parent phase with ordered vacancies. We also anticipate further theoretical investigations to elucidate the microscopic relationship between superconductivity and vacancy ordering in  $\text{Ir}_{16}\text{Sb}_{18}$ .

## I. INTRODUCTION

Vacancies and defects play crucial roles in the properties of materials, and their significance is evident in various classes of materials, including transition metal dichalcogenides (TMDs) and Fe-based superconductors. In transition metal dichalcogenides like  $\text{MoS}_2$  or  $\text{WSe}_2$ , vacancies and defects can significantly influence electronic and optical properties [3]. For instance, point defects such as sulfur or selenium vacancies can introduce localized states in the band gap, affecting the material's conductivity and optical absorption. Defects can serve as active sites for chemical reactions and play a role in catalysis [4]. Defects in TMDs can also induce magnetism and lead to interesting magnetic properties [5, 6].

Several studies have investigated the impact of vacancy ordering in different iron-based superconductors [7, 8]. For example, in iron chalcogenide superconductors such as  $\text{FeSe}$ , the ordering of selenium vacancies has

been observed to influence the electronic structure and can lead to novel phenomena, including the emergence of superconductivity [9]. Understanding and controlling the role of vacancies and defects in materials is therefore essential for tailoring their properties for specific applications. Researchers often explore the effects of defects to harness their potential benefits or mitigate undesirable consequences in various materials systems, ranging from electronics and catalysis to energy storage and superconductivity.

In this context, scientists have uncovered a distinctive type of vacancy ordering in the Ir-Sb binary system  $\text{Ir}_{16}\text{Sb}_{18}$ , manifesting as an extended buckled-honeycomb vacancy (BHV) order [1, 2]. This discovery marks a significant milestone, as  $\text{Ir}_{16}\text{Sb}_{18}$  has been identified as the first superconducting parent phase known to exhibit ordered vacancies. The emergence of superconductivity in Ir-Sb is closely linked to the suppression of the BHV ordering. This suppression is achieved through two distinct methods: high-pressure growth of  $\text{Ir}_{1-\delta}\text{Sb}$  involving the squeezing of additional Ir atoms into the vacancies, and isovalent Rh substitution  $\text{Ir}_{1-x}\text{Rh}_x\text{Sb}$ . These interventions disrupt the ordered vacancy structure, paving the

\*Electronic address: zurab.guguchia@psi.ch

way for superconductivity. However, while the connection between vacancy ordering and superconductivity is established, the exact nature of the superconducting pairing in this system remains an intriguing aspect which has not yet been fully explored.

The comprehensive exploration of superconductivity at the microscopic level in the bulk of  $\text{Ir}_{1-\delta}\text{Sb}$  and optimally doped  $\text{Ir}_{1-x}\text{Rh}_x\text{Sb}$  ( $x = 0.3$ ) is essential, requiring both experimental and theoretical investigations. In this context, our focus is on muon spin rotation/relaxation/resonance ( $\mu\text{SR}$ ) measurements of the magnetic penetration depth,  $\lambda$  in these superconductors [10, 11]. This parameter is fundamental to understanding superconductivity, as it is directly related to the superfluid density,  $n_s$  through the expression,  $1/\lambda^2 = \mu_0 e^2 n_s / m^*$  (where  $m^*$  is the effective mass). The temperature dependence of  $\lambda$  is particularly sensitive to the structure of the superconducting gap [10, 12]. Moreover, zero-field  $\mu\text{SR}$  proves to be a powerful tool for detecting a spontaneous magnetic field arising from time-reversal symmetry (TRS) breaking in exotic superconductors [13–16]. This is particularly noteworthy as internal magnetic fields as small as 0.1 G can be detected in measurements without the application of external magnetic fields. These investigations aim to unveil the intricate details of the superconducting state in  $\text{Ir}_{1-\delta}\text{Sb}$  and  $\text{Ir}_{1-x}\text{Rh}_x\text{Sb}$ , and contribute to our broader understanding of unconventional superconductivity in these materials.

We report on the fully gapped and time-reversal invariant superconducting state in the bulk of  $\text{Ir}_{1-\delta}\text{Sb}$  and  $\text{Ir}_{0.7}\text{Rh}_{0.3}\text{Sb}$ . The fully gapped nature suggests a well-defined energy structure in the superconducting state, while time-reversal invariance emphasizes the preservation of fundamental symmetries in the superconducting order parameter. The zero-temperature limit of the penetration depth was evaluated to be approximately X nm and Y nm for the respective materials. Notably, the  $T_c/\lambda_{eff}^{-2}$  ratio was found to be comparable to that of unconventional superconductors. The relatively high critical temperature ( $T_c$ ) despite a small carrier density raises the intriguing possibility of an unconventional pairing mechanism in Ir-Sb binary superconductors. This observation opens avenues for further investigation into the underlying physics of superconductivity in these materials, potentially revealing novel mechanisms that contribute to their unique superconducting properties.

## II. RESULTS AND DISCUSSION

The investigation into the possible magnetism, both static and fluctuating, in  $\text{Ir}_{1-\delta}\text{Sb}$  involved zero-field muon spin relaxation (ZF- $\mu\text{SR}$ ) experiments conducted both above and below the critical temperature,  $T_c$ . Figure 1 illustrates that, down to 1.5 K, no evidence of either static or fluctuating magnetism was detected in the ZF time spectra. The ZF- $\mu\text{SR}$  spectra were well-described by a damped Gaussian Kubo-Toyabe (GKT) depolariza-

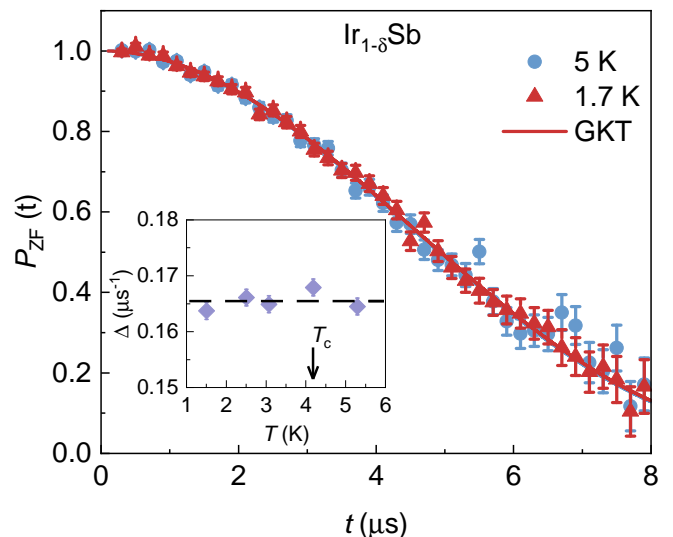


Figure 1: (Color online) **Zero-fied (ZF)  $\mu\text{SR}$  time spectra.** Time evolution of zero-field muon spin polarization, measured above and below  $T_c$  for  $\text{Ir}_{1-\delta}\text{Sb}$ , synthesized at 5.5 GPa. Error bars are the s.e.m. in about  $10^6$  events. The error of each bin count  $n$  is given by the s.d. of  $n$ . The errors of each bin in  $A(t)$  are then calculated by s.e. propagation. The solid lines represent fits to the data by means of equation (1). The inset displays the temperature dependence of the zero-field muon spin relaxation rate across  $T_c \simeq 4.0$  K.

tion function [17], indicative of the field distribution at the muon site generated by nuclear moments. Additionally, the absence of any change in the ZF- $\mu\text{SR}$  relaxation rate across  $T_c$  was observed, suggesting the lack of spontaneous magnetic fields associated with a time-reversal symmetry (TRS) breaking pairing state in  $\text{Ir}_{1-\delta}\text{Sb}$ .

Figures 2a and c depict the TF- $\mu\text{SR}$  time spectra for  $\text{Ir}_{1-\delta}\text{Sb}$  and  $\text{Ir}_{0.7}\text{Rh}_{0.3}\text{Sb}$ , respectively. These measurements were conducted in an applied magnetic field of 30 mT, both above (4 K) and below (0.08 K) the superconducting transition temperature  $T_c$ . Above  $T_c$  the oscillations show a small relaxation due to the random local fields from the nuclear magnetic moments. At 0.08 K, the relaxation rate increases due to the formation of a flux-line lattice (FLL) in the superconducting state, resulting in a nonuniform local field distribution. It is noteworthy that the rise in relaxation rate in the superconducting state is more pronounced in  $\text{Ir}_{1-\delta}\text{Sb}$  compared to  $\text{Ir}_{0.7}\text{Rh}_{0.3}\text{Sb}$ . This distinction is further evident in the Fourier transforms (see Fig. 2b and d) of the  $\mu\text{SR}$  time spectra, highlighting a significant broadening of the signal in the superconducting state for  $\text{Ir}_{1-\delta}\text{Sb}$ , whilst the spectra are almost identical below  $T_c$  in  $\text{Ir}_{0.7}\text{Rh}_{0.3}\text{Sb}$ .

As denoted by the solid lines in Figs. 2a and c, TF- $\mu\text{SR}$  data were analyzed using the following functional

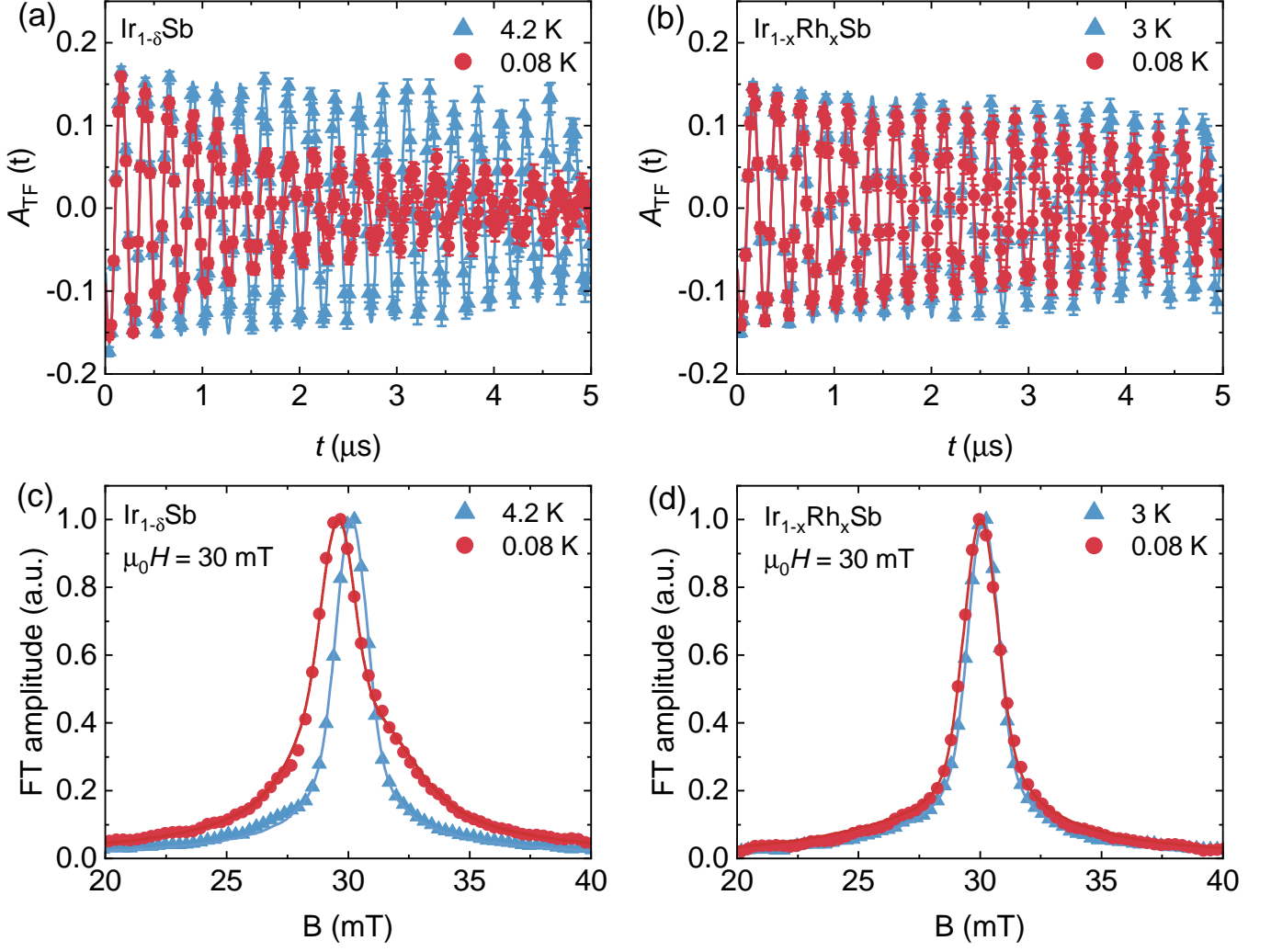


Figure 2: (Color online) **Transverse-field (TF)  $\mu$ SR time spectra and the corresponding Fourier transforms.**  $\mu$ SR spectra are obtained above and below  $T_c$  (after field cooling the sample from above  $T_c$ ) for  $\text{Ir}_{1-\delta}\text{Sb}$ , synthesized at 5.5 GPa, (a,b) and  $\text{Ir}_{1-x}\text{Rh}_x\text{Sb}$  with  $x = 0.3$  (c,d). Error bars are the s.e.m. in about  $10^6$  events. The error of each bin count  $n$  is given by the s.d. of  $n$ . The errors of each bin in  $A(t)$  are then calculated by s.e. propagation. The solid lines in (a) and (c) represent fits to the data by means of equation (3). The solid lines in (b) and (d) are the Fourier transforms of the fitted time spectra.

form [18]:

$$A_{TF_s}(t) = \sum_{i=1}^2 A_{s,i} e^{\left[ -\frac{(\sigma_{sc,i}^2 + \sigma_{nm}^2)t^2}{2} \right]} \cos(\gamma_\mu B_{int,s,i} t + \varphi). \quad (1)$$

A two-component expression was utilized for the sample  $\text{Ir}_{1-\delta}\text{Sb}$ , synthesized at 5.5 GPa, owing to the asymmetric field distribution observed (see Fig. 2c). In contrast, the field distribution for the sample  $\text{Ir}_{0.7}\text{Rh}_{0.3}\text{Sb}$  is symmetric (see Fig. 2d), hence only one component was employed. In Eq. 1,  $A_{s,i}$ ,  $B_{int,s,i}$  and  $\sigma_{sc,i}$  are the the initial asymmetry, the internal magnetic field at the muon site and the superconducting relaxation rates of the  $i$ -th component.  $\sigma_{nm}$  characterizes the damping due to the nuclear magnetic dipolar contribution. During the analysis  $\sigma_{nm}$  was assumed to be constant over the entire temperature range and was fixed to the value obtained above

$T_c$  where only nuclear magnetic moments contribute to the muon depolarization rate. In order to extract superconducting muon spin depolarization rate  $\sigma_{sc}$  (the second moment of the field distribution) and  $B_{int,s}$  (the first moment of the field distribution) from the two-component fitting we used the same procedure as described in Ref. [19].

In Fig. 2a,  $\sigma_{sc}$  is plotted against temperature for both  $\text{Ir}_{1-\delta}\text{Sb}$ , synthesized at 5.5 GPa (at  $\mu_0 H = 0.03$  T), and for  $\text{Ir}_{0.7}\text{Rh}_{0.3}\text{Sb}$  (at  $\mu_0 H = 0.01$  T and 0.03 T). Below  $T_c$ , the relaxation rate  $\sigma_{sc}$  begins to increase from zero due to the formation of the flux-line lattice (FLL) and exhibits saturation at lower temperatures. The temperature dependence of  $\sigma_{sc}$  reflects the topology of the superconducting gap and is consistent with the presence of a single superconducting gap on the Fermi surface of these materials, as we show below. The absolute value

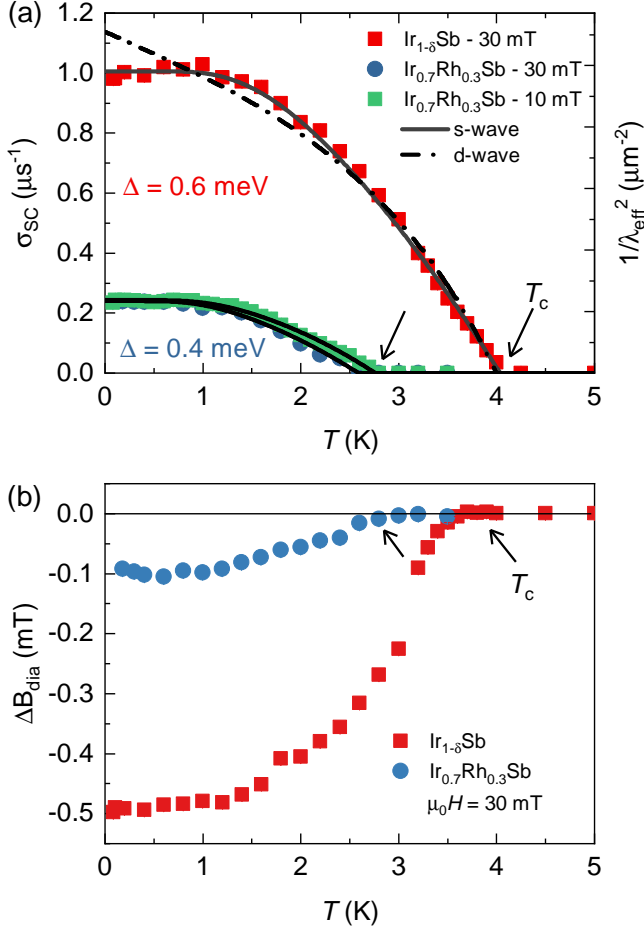


Figure 3: (Color online) **Superconducting muon spin depolarization rate  $\sigma_{sc}$  and the field shift.** (a) Temperature dependence of the superconducting muon spin depolarization rate,  $\sigma_{sc}$  measured in an applied magnetic fields of  $\mu_0 H = 10$  mT and 30 mT for  $Ir_{1-\delta}Sb$ , synthesized at 5.5 GPa and  $Ir_{1-x}Rh_xSb$  with  $x = 0.3$ . (b) Temperature dependence of the difference between the internal field  $\mu_0 H_{SC}$  measured in the SC state and the one measured in the normal state  $\mu_0 H_{NS}$  at  $T = 5$  K for  $Ir_{1-\delta}Sb$  and  $Ir_{1-x}Rh_xSb$ .

of  $\sigma_{sc}$  is five times smaller for  $Ir_{0.7}Rh_{0.3}Sb$  compared to  $Ir_{1-\delta}Sb$ , indicating a lower superfluid density for the Rh-doped sample. Below  $T_c$ , a large diamagnetic shift of  $B_{int,s}$  experienced by the muons is observed in both samples. In Fig. 2b, the temperature dependence of the diamagnetic shift  $\delta B_{dia} = B_{int,s,SC} - B_{int,s,NS}$  is plotted, where  $B_{int,s,SC}$  represents the internal field measured in the superconducting state, and  $B_{int,s,NS}$  is the internal field measured in the normal state at 5 K. This diamagnetic shift indicates the bulk nature of superconductivity and rules out the possibility of field-induced magnetism in these superconductors.

To perform a quantitative analysis, it is important to note that the London magnetic penetration depth  $\lambda(T)$  is directly related to the measured relaxation rate in the superconducting state  $\sigma_{sc}$ . For triangular FLL

relationship is described by the equation [20]:

$$\frac{\sigma_{sc}^2(T)}{\gamma_\mu^2} = 0.00371 \frac{\Phi_0^2}{\lambda^4(T)}, \quad (2)$$

where  $\Phi_0 = 2.068 \times 10^{-15}$  Wb is the magnetic-flux quantum. Equation (2) is applicable only when the separation between vortices is smaller than  $\lambda$ . In this particular scenario, as per the London model,  $\sigma_{sc}$  becomes field-independent [20].

To explore the superconducting gap structure of  $Ir_{1-\delta}Sb$  and  $Ir_{0.7}Rh_{0.3}Sb$ , we conducted an analysis of the temperature dependence of the magnetic penetration depth,  $\lambda(T)$ , directly linked to the superconducting gap. The behavior of  $\lambda(T)$  can be characterized within the local (London) approximation ( $\lambda \gg \xi$ ) using the following expression [18, 21]:

$$\frac{\lambda^{-2}(T, \Delta_{0,i})}{\lambda^{-2}(0, \Delta_{0,i})} = 1 + \frac{1}{\pi} \int_0^{2\pi} \int_{\Delta(T,\varphi)}^{\infty} \left( \frac{\partial f}{\partial E} \right) \frac{E dE d\varphi}{\sqrt{E^2 - \Delta_i(T, \varphi)^2}}, \quad (3)$$

where  $f = [1 + \exp(E/k_B T)]^{-1}$  is the Fermi function,  $\varphi$  is the angle along the Fermi surface, and  $\Delta_i(T, \varphi) = \Delta_{0,i} \Gamma(T/T_c) g(\varphi)$  ( $\Delta_{0,i}$  is the maximum gap value at  $T = 0$ ). The temperature dependence of the gap is approximated by the expression  $\Gamma(T/T_c) = \tanh\{1.82[1.018(T_c/T - 1)]^{0.51}\}$ , [22] while  $g(\varphi)$  describes the angular dependence of the gap and it is replaced by 1 for both an *s*-wave gap,  $[1 + \cos(4\varphi)]/(1+a)$  for an anisotropic *s*-wave gap and  $|\cos(2\varphi)|$  for a *d*-wave gap [23].

In Fig 3a, the experimentally obtained  $\lambda_{eff}^{-2}(T)$  dependence is most accurately described by a momentum-independent *s*-wave model with a gap value of  $\Delta = 0.6(1)$  meV and  $T_c = 4.1(1)$  K for  $Ir_{1-\delta}Sb$ , and a gap value of  $\Delta = 0.4(1)$  meV and  $T_c = 2.7(2)$  K for  $Ir_{0.7}Rh_{0.3}Sb$ . The *d*-wave and *p*-wave gap symmetries were also considered but were found to be inconsistent with the data (illustrated by the dashed line in Fig. 3a). Particularly, these models struggle to account for the very weak temperature dependence of  $\lambda(T)$  at low temperatures. Additionally, the power-law behavior  $\left[1 - \left(\frac{T}{T_c}\right)^2\right]$ , theoretically proposed for the superfluid density of dirty *d*-wave superconductors [24], was tested but deemed inconsistent with the data. This analysis shows that a nodeless or fully gapped state is the most plausible bulk superconducting pairing state for  $Ir_{1-\delta}Sb$  and  $Ir_{0.7}Rh_{0.3}Sb$ .

The estimated ratio of the superconducting gap to  $T_c$ ,  $(2\Delta/k_B T_c)$ , is approximately 3.4, aligning with the BCS (Bardeen-Cooper-Schrieffer) expectation [10]. However, it's crucial to acknowledge that a similar ratio can also be anticipated within a Bose-Einstein Condensation (BEC)-like framework. Importantly, the ratio  $2\Delta/k_B T_c$ , on its own, does not effectively distinguish between BCS or BEC condensation scenarios. Further insights are required to differentiate between these two possibilities and

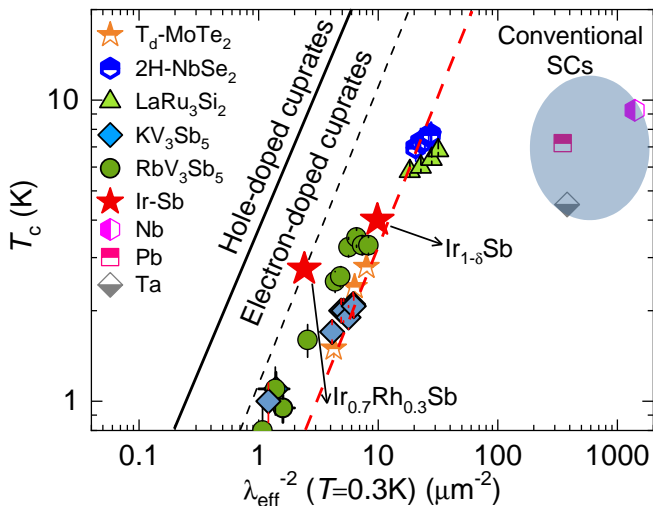


Figure 4: (Color online) **Hallmark feature of unconventional superconductivity.** Plot of  $T_c$  versus  $\lambda_{\text{eff}}^{-2}(0)$  on a logarithmic scale obtained from  $\mu\text{SR}$  experiments for  $\text{Ir}_{1-\delta}\text{Sb}$ , synthesized at 5.5 GPa and  $\text{Ir}_{0.7}\text{Rh}_{0.3}\text{Sb}$ . The data for the kagome-lattice superconductors  $\text{KV}_3\text{Sb}_5$  [15, 16, 35],  $\text{RbV}_3\text{Sb}_5$  [35], and  $\text{LaRu}_3\text{Si}_2$  [36] are also included. The dashed red line represents the relationship obtained for the layered transition metal dichalcogenide superconductors,  $T_d\text{-MoTe}_2$  and  $2\text{H-NbSe}_2$  by Guguchia *et al.* [34, 40]. The relationship observed for cuprates is shown [31, 33] as well as the points for various conventional superconductors.

elucidate the nature of the superconducting state in the studied materials. What distinguishes between BCS and BEC superconductivity is a key parameter: the ratio of the superconducting critical temperature to the superfluid density. This ratio,  $T_c/n_s$ , plays a crucial role in characterizing the nature of the superconducting state in different materials. In a simplified interpretation of the BEC to BCS crossover, the  $T_c/n_s$  ratio serves as a critical parameter. Systems characterized by a small  $T_c/n_s$  (with a large superfluid density,  $n_s$ ) are often considered to reside on the "BCS" side of the crossover. Conversely, systems with a large  $T_c/n_s$  (exhibiting a small superfluid density,  $n_s$ ) are expected to be on the BEC side. Moreover, the correlation between  $T_c$  and the superfluid density is anticipated to be significant primarily on the BEC side of the crossover. As one moves from the BCS limit to the BEC limit in the crossover, the nature of the pairing mechanism evolves, transitioning from Cooper pairs formed through electron-phonon interactions (BCS) to a more Bose-Einstein condensation-like scenario involving preformed pairs.

The observation of a correlation between  $T_c$  and the superfluid density ( $\lambda_{\text{eff}}^{-2}$ ) was first noted in hole-doped cuprates back in 1988-89 [31, 32], extending later to include electron-doped cuprates [33]. This intriguing relationship has been investigated across various superconducting systems. Guguchia and collaborators demonstrated that this linear correlation is an intrinsic

feature in superconductors such as transition metal dichalcogenides [10, 34] and kagome-lattice superconductors [15, 35, 40]. The ratio  $T_c/\lambda_{\text{eff}}^{-2}$  in these systems tends to be lower than that observed in hole-doped cuprates (see Figure 4). To contextualize the superconductors  $\text{Ir}_{1-\delta}\text{Sb}$  and  $\text{Ir}_{0.7}\text{Rh}_{0.3}\text{Sb}$  within this framework, Fig. 4 illustrates the critical temperature plotted against the superfluid density. For  $\text{Ir}_{0.7}\text{Rh}_{0.3}\text{Sb}$ , the estimated ratio  $T_c/\lambda_{\text{eff}}^{-2}$  is approximately 1, closely resembling electron-doped cuprates known for their correlated superconductivity. In the case of  $\text{Ir}_{1-\delta}\text{Sb}$ , the ratio is reduced to 0.4 but remains notably distant from conventional BCS superconductors. Intriguingly, it aligns nearly perfectly with the trend line occupied by charge density wave superconductors like  $2\text{H-NbSe}_2$ ,  $4\text{H-NbSe}_2$ ,  $\text{LaRu}_3\text{Si}_2$ , as well as the Weyl-superconductor  $T_d\text{-MoTe}_2$  [10]. This finding strongly suggests an unconventional pairing mechanism in  $\text{Ir}_{1-\delta}\text{Sb}$  and  $\text{Ir}_{0.7}\text{Rh}_{0.3}\text{Sb}$ , characterized by a low density of Cooper pairs.

Another unconventional feature in the superconducting phase diagram of  $\text{Ir}_{1-x}\text{Rh}_x\text{Sb}$  is a dome-shaped dependence of  $T_c$  (see Figure 5a). This pattern is characterized by an optimal  $T_c$  value occurring at  $x = 0.3$ , followed by a reduction as the Rh concentration deviates from this optimal point. The isovalent Rh substitution on the Ir site in IrSb, without introducing additional holes or electrons, creates a condition often termed "chemical pressure". Typically, chemical substitution introduces disorder effects, potentially influencing  $T_c$ . To discern the intrinsic nature of this dome shape, a cleaner external parameter is essential. For example, hydrostatic pressure introduces fewer disorder effects compared to isovalent chemical substitutions ("chemical pressure"). For this reason, we explored the impact on  $T_c$  in the optimally Rh-doped,  $\text{Ir}_{0.7}\text{Rh}_{0.3}\text{Sb}$  with hydrostatic pressure, spanning a range up to  $p = 2.2$  GPa. As shown in Figs. 5b and c, the observed trend revealed a linear decrease in  $T_c$  with increasing pressure. This behavior aligns closely with the effects of Rh doping. This finding suggests that the impact of both external pressure conditions applied hydrostatically and induced through chemical modifications is consistent in the  $\text{Ir}_{0.7}\text{Rh}_{0.3}\text{Sb}$  system. This highlights the intrinsic nature of the reduction in  $T_c$  beyond  $x = 0.3$  and enhance our understanding of the unique aspects of superconductivity in this material.

### III. CONCLUSIONS

In summary, our study provides a microscopic exploration of superconductivity in  $\text{Ir}_{1-\delta}\text{Sb}$  (synthesized at 5.5 GPa with  $T_c = 4.2$  K) and optimally Rh-doped  $\text{Ir}_{0.7}\text{Rh}_{0.3}\text{Sb}$  ( $T_c = 2.7$  K) in close proximity to vacancy ordering, employing a bulk sensitive local probe. Specifically, we investigated the zero-temperature magnetic penetration depth  $\lambda_{\text{eff}}(0)$  and the temperature dependence of  $\lambda_{\text{eff}}^{-2}$  through  $\mu\text{SR}$  experiments. The superfluid density in both systems aligns with a scenario of

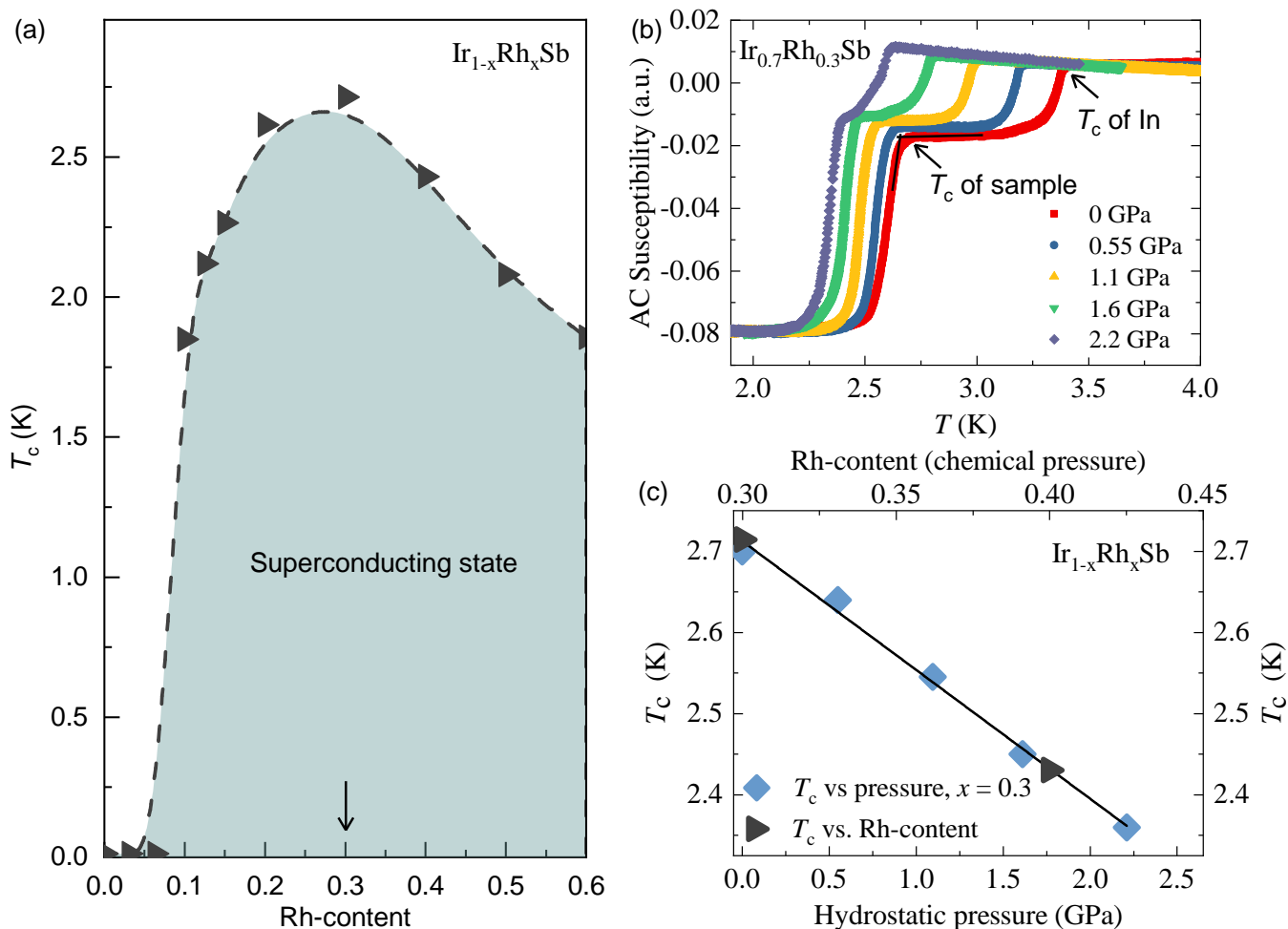


Figure 5: (Color online) **Chemical and hydrostatic pressure effects on superconductivity in  $\text{Ir}_{1-x}\text{Rh}_x\text{Sb}$ .** (a) The superconducting critical temperature vs Rh-content, showing a dome-shaped SC phase diagram (adapted from Ref. [1]). Arrows indicate the sample with  $x = 0.3$ , which was measured under hydrostatic pressure. (b) The temperature dependence of AC susceptibility, measured at various hydrostatic pressure, ranging up to 2.21 GPa. (c) The superconducting critical temperature as a function of hydrostatic pressure and the Rh-content ("chemical pressure") in the range between  $x = 0.3$  and 0.45.

a complete gap. Intriguingly, the  $T_c/\lambda_{eff}^{-2}$  ratio is comparable to that of high-temperature unconventional superconductors, suggesting the unconventional nature of superconductivity in Ir-Sb binary superconductors. Additionally, the  $\mu\text{SR}$  experiments, serving as an extremely sensitive magnetic probe, do not exhibit evidence of spontaneous magnetic fields, which would be expected for a time-reversal-symmetry-breaking state in the bulk of the superconductor. Consequently, our results categorize  $\text{Ir}_{1-\delta}\text{Sb}$  and  $\text{Ir}_{0.7}\text{Rh}_{0.3}\text{Sb}$  as unconventional, time-reversal-invariant, and fully gapped bulk superconductors. We further demonstrate the striking similarity between the effects of chemical pressure, induced by isovalent Rh substitution, and hydrostatic pressure on the superconducting critical temperature in  $\text{Ir}_{0.7}\text{Rh}_{0.3}\text{Sb}$ . This highlights that the observed dome-shaped dependence of  $T_c$  is not merely a consequence of disorder effects introduced by chemical substitution but is rooted in the intrinsic properties of the material. These results offer valu-

able insights into the underlying mechanisms governing the material's behavior. A more comprehensive analysis requires consideration of various factors, including the specific pairing mechanisms and the role of interactions in the superconducting state.

#### IV. ACKNOWLEDGMENTS

The  $\mu\text{SR}$  experiments were carried out at the Swiss Muon Source ( $S\mu\text{S}$ ) Paul Scherrer Institute, Villigen, Switzerland. Z.G. acknowledges support from the Swiss National Science Foundation (SNSF) through SNSF Starting Grant (No. TMSGI2\_211750). Z.G. acknowledges the useful discussions with Robert Scheuermann. T.Y. would like to acknowledge Beijing Natural Science Foundation (Grant No. Z200005).

**Author Contributions:** Z. Guguchia conceived and

supervised the project. Sample Growth: Y.P. and H.H..  $\mu$ SR experiments, data analysis and corresponding discussions: V.S., J.N.G., D.D., C.M.III., S.S.I., R.K., H.L., and Z.G.. Figure development and writing of the paper: Z.G., and V.S., with contributions from all authors. All authors discussed the results, interpretation and conclusion.

**Competing interests:** The authors declare that they have no competing interests.

## V. METHODS

**Sample growth:** The details of the synthesis of the polycrystalline samples of  $\text{Ir}_{1-\delta}\text{Sb}$  and  $\text{Ir}_{0.7}\text{Rh}_{0.3}\text{Sb}$  are reported elsewhere [1, 2].

**Experimental details:** Zero field (ZF) and transverse field (TF)  $\mu$ SR experiments were performed on

the GPS ( $\pi$ M3 beamline) [37], and high-field HAL-9500 instruments ( $\pi$ E3 beamline) [38], equipped with Blue-Fors vacuum-loaded cryogen-free dilution refrigerator (DR), at the Swiss Muon Source ( $S\mu$ S) at the Paul Scherrer Institute, in Villigen, Switzerland. Zero field is dynamically obtained (compensation better than 30 mG) by a newly installed automatic compensation device [37]. When performing measurements in zero-field the geomagnetic field or any stray fields are tabulated and automatically compensated by the automatic compensation device. The  $\mu$ SR time spectra were analyzed using the free software package MUSRFIT [18]. AC susceptibility experiments under pressure were carried out using double wall piston-cylinder type of cell made of MP35N/MP35N material generate pressures up to 2.3 GPa [39–41]. A small indium plate was placed together with the sample in the pressure cell filled with the Daphne oil. The pressure was estimated by tracking the SC transition of a indium plate by AC susceptibility.

- 
- [1] Qi, Y. et al. Superconductivity from buckled-honeycomb-vacancy ordering. *Science Bulletin* **66**, 327-331 (2021).
- [2] Ying, T. et al. Fermi surface nesting, vacancy ordering and the emergence of superconductivity in IrSb compounds. arXiv:2108.13704 (2021).
- [3] C. Ataca et. al., Mechanical and Electronic Properties of  $\text{MoS}_2$  Nanoribbons and Their Defects. *J. Phys. Chem. C* **115**, 3934-3941 (2011).
- [4] Y. Luo et. al., Defect Engineering of Nanomaterials for Catalysis. *Nanomaterials* **13(6)**, 1116 (2023).
- [5] Z. Guguchia et. al., Magnetism in Semiconducting Molybdenum Dichalcogenides. *Sci. Adv.* **4**: eaat3672 (2018).
- [6] S. Tongay, et. al., Magnetic properties of  $\text{MoS}_2$ : Existence of ferromagnetism. *Appl. Phys. Lett.* **101**, 123105 (2012).
- [7] Y. Fang et. al., Fe-vacancy ordering in superconducting  $\text{K}_{1-x}\text{Fe}_{2-y}\text{Se}_2$ : first-principles calculations and Monte Carlo simulations. *Supercond. Sci. Technol.* **28**, 095004 (2015).
- [8] A.M. Zhang et. al., Vacancy ordering and phonon spectrum of the iron-based superconductor  $\text{K}_{0.8}\text{Fe}_{1.6}\text{Se}_2$ . *Phys. Rev. B* **85**, 024518 (2012).
- [9] T.K. Chen et. al., Fe-vacancy order and superconductivity in tetragonal  $\text{Fe}_{1-x}\text{Se}$ . *PNAS* **111**, 63768 (2014).
- [10] Guguchia, Z. et al. Signatures of the topological  $s^{+-}$  superconducting order parameter in the type-II Weyl semimetal  $T_d\text{-MoTe}_2$ . *Nature Communications* **8**, 1082 (2017).
- [11] J. E. Sonier, J. H. Brewer, and R. F. Kiefl, *Reviews of Modern Physics* **72**, 769 (2000).
- [12] Das, D. et al., Unconventional Pressure Dependence of the Superfluid Density in the Nodeless Topological Superconductor  $\alpha\text{-PdBi}_2$ . *Phys. Rev. Lett.* **127**, 217002 (2021).
- [13] G.M. Luke, et al. Time-reversal symmetrybreaking superconductivity in  $\text{Sr}_2\text{RuO}_4$ . *Nature* **394**, 559 (1998).
- [14] Hillier, A.D., Jorge, Q., and Cywinski, R. Evidence for Time-Reversal Symmetry Breaking in the Noncentrosymmetric Superconductor  $\text{LaNiC}_2$ . *Phys. Rev. Lett.* **102**, 117007 (2009).
- [15] Guguchia, Z., Khasanov, R. and Luetkens, H. Unconventional charge order and superconductivity in kagome-lattice systems as seen by muon-spin rotation. *npj Quantum Materials* **8**, 41 (2023).
- [16] Mielke III, C. et al., and Guguchia, Z. Time-reversal symmetry-breaking charge order in a kagome superconductor. *Nature* **602**, 245-250 (2022).
- [17] R. Kubo and T. Toyabe, In *Magnetic Resonance and Relaxation*, ed. R. Blinc (North-Holland, Amsterdam, 1967) p. 810; T. Toyabe, M.S. thesis, University of Tokyo (1966).
- [18] *Physics Procedia* **30**, 69 (2012). The fitting of Eq. 4 was performed using the additional library BMW developed by B. Wojek.
- [19] Khasanov, R. et al., Experimental Evidence for Two Gaps in the High Temperature  $\text{La}_{1.83}\text{Sr}_{0.17}\text{CuO}_4$  Super-

- conductor. *Phys. Rev. Lett.* **98**, 057007 (2007).
- [20] E.H. Brandt, *Phys. Rev. B* **37**, 2349 (1988).
- [21] M. Tinkham, Introduction to Superconductivity, Krieger Publishing Company, Malabar, Florida, 1975.
- [22] A. Carrington and F. Manzano, *Physica C* **385**, 205 (2003).
- [23] M.H. Fang, H.M. Pham, B. Qian, T.J. Liu, E.K. Vehstedt, Y. Liu, L. Spinu, and Z.Q. Mao, *Phys. Rev. B* **78**, 224503 (2008).
- [24] P.J. Hirschfeld, W.O. Putikka, and D.J. Scalapino, *d*-wave Model for Microwave Response of High- $T_c$  Superconductors. *Phys. Rev. B* **50**, 10250 (1994).
- [25] R. Khasanov, A. Shengelaya, K. Conder, E. Morenzoni, I. M. Savic, J. Karpinski, and H. Keller, *Phys. Rev. B* **74**, 064504 (2006).
- [26] H. Luetkens, H.-H. Klauss, R. Khasanov, A. Amato, R. Klingeler, I. Hellmann, N. Leps, A. Kondrat, C.Hess, A. Kohler, G. Behr, J. Werner, and B. Buchner. *Phys. Rev. Lett.* **101**, 097009 (2008).
- [27] J.E. Sonier, *Journal of the Physical Society of Japan* **85**, 091005 (2016)
- [28] D.R. Harshman, A.T. Fiory, *J. Phys.: Condens. Matter* **23**, 315702 (2011).
- [29] H. Leng, D. Cherian, Y. K. Huang, J.-C. Orain, A. Amato, and A. de Visser, *Phys. Rev. B* **97**, 054503 (2018).
- [30] P. Neha, P. K. Biswas, Tanmoy Das, and S. Patnaik, *Phys. Rev. Materials* **3**, 074201 (2019).
- [31] Uemura, Y.J. et. al., Universal Correlations between  $T_c$  and  $n_s/m^*$  (Carrier Density over Effective Mass) in High- $T_c$  Cuprate Superconductors. *Phys. Rev. Lett.* **62**, 2317 (1989).
- [32] Uemura, Y.J. et. al., Basic Similarities among Cuprate, Bismuthate, Organic, Chevrel Phase, and Heavy-Fermion Superconductors Shown by Penetration Depth Measurements. *Phys. Rev. Lett.* **66**, 2665 (1991).
- [33] Shengelaya, A. et al. Muon-Spin-Rotation Measurements of the Penetration Depth of the Infinite-Layer Electron-Doped  $\text{Sr}_{0.9}\text{La}_{0.1}\text{CuO}_2$  Cuprate Superconductor. *Phys. Rev. Lett.* **94**, 127001 (2005).
- [34] von Rohr, F. O. et al. Unconventional Scaling of the Superfluid Density with the Critical Temperature in Transition Metal Dichalcogenides. *Science Advances* **5**(11), eaav8465 (2019).
- [35] Guguchia, Z. et al., Tunable unconventional kagome superconductivity in charge ordered  $\text{RbV}_3\text{Sb}_5$  and  $\text{KV}_3\text{Sb}_5$ . *Nature Communications* **14**, 153 (2023).
- [36] Mielke III, C. et al. and Guguchia, Z. Nodeless kagome superconductivity in  $\text{LaRu}_3\text{Si}_2$ . *Phys. Rev. Mat.* **5**, 034803 (2021).
- [37] A. Amato, et. al., The new versatile general purpose surface-muon instrument (GPS) based on silicon photomultipliers for  $\mu\text{SR}$  measurements on a continuous-wave beam. *Rev. Sci. Instrum.* **88**, 093301 (2017).
- [38] Sedlak, K., Scheuermann, R., Stoykov, A., Amato, A. GEANT4 simulation and optimisation of the high-field  $\mu\text{SR}$  spectrometer. *Physica B* **404**, 970-973 (2009).
- [39] R. Khasanov, Z. Guguchia, A. Maisuradze, D. Andreica, M. Elender, A. Raselli, Z. Shermadini, T. Goko, F. Knecht, E. Morenzoni, and A. Amato, High pressure research using muons at the Paul Scherrer Institute. *High Pressure Research* **36**, 140-166 (2016).
- [40] Z. Guguchia, et. al., Direct evidence for the emergence of a pressure induced nodal superconducting gap in the iron-based superconductor  $\text{Ba}_{0.65}\text{Rb}_{0.35}\text{Fe}_2\text{As}_2$ . *Nature Communications* **6**, 8863 (2015).
- [41] R. Khasanov. Perspective on the muon-spin rotation/relaxation under hydrostatic pressure. *Journal of Applied Physics* **132**, 190903 (2022).